

L2M-Reg: Building-level Uncertainty-aware Registration of Outdoor LiDAR Point Clouds and Semantic 3D City Models

Ziyang Xu^{*a}, Benedikt Schwab^b, Yihui Yang^a, Thomas H. Kolbe^b, Christoph Holst^a

^a*Chair of Engineering Geodesy, Technical University of Munich, Munich, 80333, Germany*

^b*Chair of Geoinformatics, Technical University of Munich, Munich, 80333, Germany*

Abstract

Accurate registration between LiDAR (Light Detection and Ranging) point clouds and semantic 3D city models is a fundamental topic in urban digital twinning and a prerequisite for downstream tasks, such as digital construction, change detection and model refinement. However, achieving accurate LiDAR-to-Model registration at individual building level remains challenging, particularly due to the generalization uncertainty in semantic 3D city models at the Level of Detail 2 (LoD2). This paper addresses this gap by proposing L2M-Reg, a plane-based fine registration method that explicitly accounts for model uncertainty. L2M-Reg consists of three key steps: establishing reliable plane correspondence, building a pseudo-plane-constrained Gauss–Helmert model, and adaptively estimating vertical translation. Experiments on three real-world datasets demonstrate that L2M-Reg is both more accurate and computationally efficient than existing ICP-based and plane-based methods. Overall, L2M-Reg provides a novel building-level solution regarding LiDAR-to-Model registration when model uncertainty is present.

Keywords: Urban digital twinning, Point cloud registration, CityGML, Data fusion, Digital construction

1. Introduction

LiDAR (Light Detection and Ranging) point clouds and semantic 3D city models are two widely used digital representations that play important roles in urban digital twinning (Jeddoub et al., 2023; Ketzler et al., 2020). However, as heterogeneous data types, they differ in many aspects such as data format, acquisition methods, geometric features, and accuracy. Specifically, semantic 3D city models primarily contain generalized structural information and serve as simplified and abstract representations of physical buildings, whereas LiDAR point clouds accurately capture detailed geometric features, providing high-precision representations (Kada and McKinley, 2009; Xu and Stilla, 2021). Accurate and efficient registration between them constitutes a fundamental research topic, as well as an essential prerequisite for numerous downstream applications such as digital construction, change detection, model updating and enrichment, model reconstruction and texturing (Liu et al., 2024; Shao et al., 2024; Zhu et al., 2024; Wysocki et al., 2021; Kulmer et al., 2025).

Internationally, CityGML (City Geography Markup Language), as a standard developed by the Open Geospatial Consortium (OGC), is widely adopted for representing

*Corresponding author.

Email addresses: ziyang.xu@tum.de (Ziyang Xu*), yihui.yang@tum.de (Yihui Yang)

and managing semantic 3D city models (Kolbe et al., 2021; Gröger and Plümer, 2012). CityGML supports the modeling of urban objects by incorporating their 3D geometry, appearance, topology, and semantic information across four distinct Levels of Details (LoD) (Kolbe et al., 2021). Benefiting from the widespread adoption of CityGML, accurately georeferenced LoD2 models are publicly available in many countries and regions (Wysocki et al., 2024). These models are typically maintained by governmental agencies or professional institutions to ensure consistent quality and reliability. Consequently, in most LiDAR-to-Model registration tasks, existing georeferenced LoD2 models are utilized as reference data, to which up-to-date LiDAR point clouds are aligned.

When discussing LoD2 building models used for accurate registration, a particularly critical issue is their inherent uncertainty. The encountered uncertainty stems from the current model generation process, which typically relies on 2D building footprints from the cadastral registry. As illustrated in Figure 1, the building footprint is defined by the outermost structural elements.

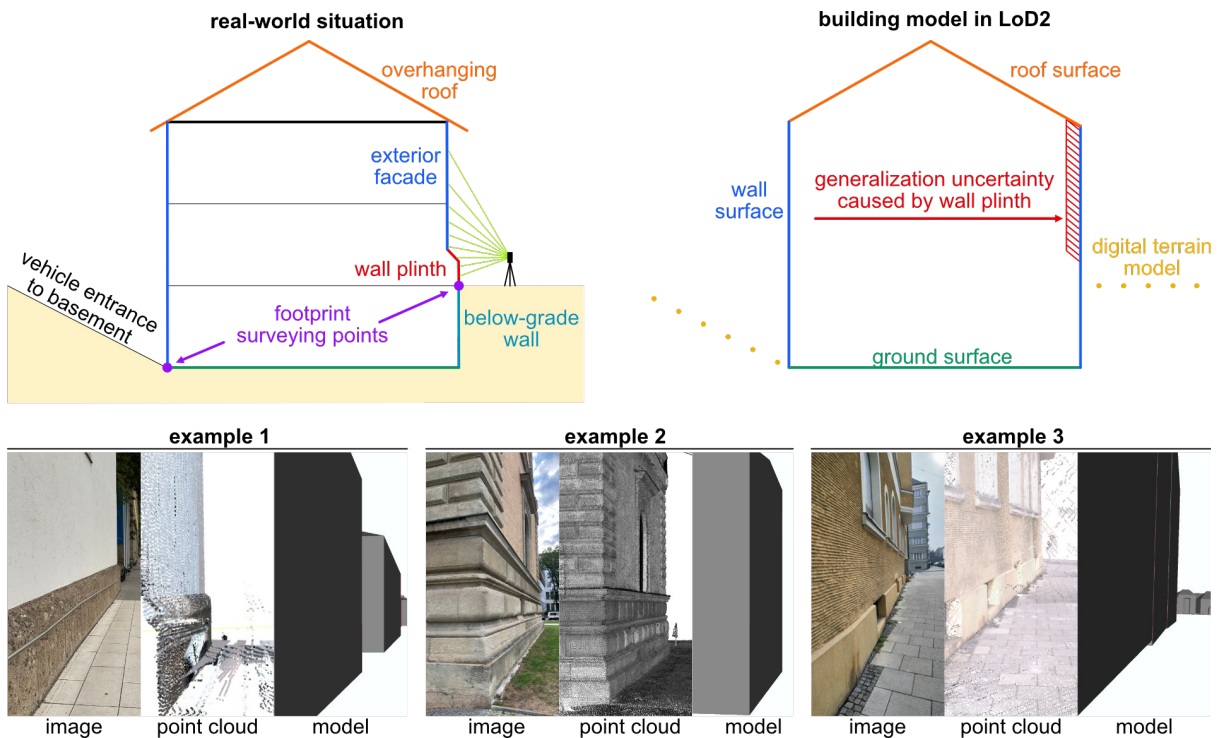


Figure 1: Sources of uncertainty in LoD2 building models. Model uncertainty primarily arises from the model generation process. In reality, building footprint points correspond to the wall plinth rather than the upper facade, resulting in a horizontal offset between the two (as indicated by the red dashed area). Since LoD2 models are generated directly from these footprint points, the modeled wall surfaces align geometrically with the plinth, but not with the actual facade above.

As seen in Figure 1, buildings typically consist of various structural elements from the foundation to the roof, such as wall plinth (in red), exterior facade (in blue), and overhanging roof (in orange). Cadastral surveying regulations define which of these elements should be included in the model. Typically, a horizontal offset exists between a building’s plinth and its upper facade. Depending on the architectural style, this offset can range from several centimeters to decimeters. Since LoD2 building models are generally reconstructed by extruding building footprints to prototypical roof shapes from Airborne Laser Scanning (ALS) data (Roschlaub and Batscheider, 2016), the modeled wall surfaces actually only align with the building’s plinths, not facades. Consequently, the building

plinths that closely correspond to footprint should be more suited for establishing correspondences with modeled wall surfaces.

Previous studies on LiDAR-to-Model registration have commonly assumed that the LoD2 models served as reference data are error-free, thus neglecting this inherent uncertainty. Although this assumption is basically accepted, it will become problematic in high-precision application scenarios. For example, when the captured LiDAR point clouds need to be accurately georeferenced based on existing LoD2 models, this horizontal offset between the plinth and exterior facade cannot be disregarded. Recent research has acknowledged similar issues about model uncertainty, focusing primarily on visual and conceptual representations from architectural or modeling perspectives (Landes et al., 2019; Potter et al., 2012; Zou and Sester, 2022). However, most LiDAR-to-Model registration studies have overlooked this uncertainty issue, treating it as a conventional point cloud registration task. As a result, a disconnection arises between building modeling and LiDAR-to-Model registration research.

Since urban dwellings form the backbone of any city, most existing semantic 3D city models are composed of buildings (Biljecki et al., 2015). Compared to city-level LiDAR-to-Model registration, accurate and efficient building-level solution offers the potential to refine city models based on specific needs, thereby avoiding extensive data acquisition and substantially reducing costs. However, this transition introduces several challenges:

- (1) **Increased accuracy requirements.** Inherent model uncertainty that is negligible at the city scale needs to be explicitly addressed at the building level for high-precision applications.
- (2) **Limited availability of geometric features.** Individual buildings or partial building segments typically contain fewer geometric primitives—such as facade planes—with limited diversity in orientation and quantity. This constraint makes feature extraction and correspondence establishment more difficult.
- (3) **Demand for balanced accuracy and efficiency.** While high accuracy is essential, efficient processing at the building level is equally important to enable scalability for city-scale applications.

These challenges underscore a clear research gap in achieving accurate building-level LiDAR-to-Model registration under model uncertainty. In this context, model uncertainty is defined as the inconsistency between the final model, produced through a predefined generation process, and the actual building object, specifically in terms of geometric and structural representation. To address this, a tailored solution named L2M-Reg is proposed. To the best of our knowledge, this is the first comprehensive study to explicitly account for the inherent uncertainty of reference LoD2 models in building-level registration. The main contributions are summarized as follows:

- (1) A plane-based LiDAR-to-Model fine registration method, L2M-Reg, tailored for individual buildings is proposed. It integrates reliable plane correspondence establishment, pseudo-plane-constraint Gauss-Helmert Model (GHM), and adaptable vertical translation estimation. By explicitly considering the uncertainty in LoD2 models, L2M-Reg achieves superior performance on three real-world datasets.
- (2) A 2D-3D decoupled transformation parameter estimation strategy is introduced to mitigate the adverse impact of low-quality ground model data on the overall accuracy of 6 Degree-of-Freedom (DoF) parameter estimation. By decoupling vertical

and horizontal components, this strategy effectively prevents high ground model uncertainty from degrading horizontal registration accuracy.

- (3) A lightweight plane correspondence strategy is developed that leverages the embedded semantic information in LoD2 models. It eliminates the conventional need for converting models into point clouds and performing feature-based matching, thereby significantly improving robustness and computational efficiency. Furthermore, it is built upon the internationally recognized CityGML standard, ensuring high interoperability and ease of adoption across different countries and regions.

This paper starts with a background introduction on LiDAR-to-Model registration and the inherent uncertainty of LoD2 models, followed by a detailed review of related works in Section 2. Section 3 presents the detailed methodology of L2M-Reg. Section 4 describes the experimental results. Section 5 discusses the advantages and limitations, followed by conclusions and outlook in Section 6.

2. Related Works

This paper focuses on accurate LiDAR-to-Model registration while explicitly accounting for the inherent uncertainty in LoD2 models. Thus, the related work is divided into LiDAR-to-Model registration (Section 2.1) and the inherent uncertainty of models (Section 2.2).

2.1. LiDAR-to-Model Registration

Accurate registration between LiDAR point clouds and LoD2 models is an essential and fundamental task. In recent years, researchers worldwide have extensively investigated this topic, which can be summarized into two categories: registration directly using LoD2 models in Section 2.1.1 and registration using converted point clouds from LoD2 models in Section 2.1.2 (Bueno et al., 2018; Sheik et al., 2022a).

2.1.1. Registration Directly Using LoD2 Models

The registration between LiDAR point clouds and their corresponding LoD2 models essentially involves feature extraction and correspondence matching across heterogeneous data. A straightforward strategy to address this issue is to directly extract geometric features, such as points, lines, and planes, from the models and subsequently match these features with corresponding ones derived from the point clouds (Bueno et al., 2018; Sheik et al., 2022a,b; Monasse et al., 2023; Bosché, 2012; Lucks et al., 2021; Goebbels et al., 2019). The transformation parameters can then be computed based on these matched features. In particular, most man-made structures include numerous planar surfaces, which naturally facilitates the extraction and utilization of planar features (Sheik et al., 2022a; Qiao and Butt, 2023).

Another strategy is to use the footprint points or polygons of the entire model as features to calculate the rotation and translation parameters (Diakite and Zlatanova, 2020). However, methods relying on footprint points or polygon-based strategies encounter difficulties when dealing with symmetrical buildings, as these methods cannot accurately estimate the rotation parameters of entirely symmetrical structures and may introduce ambiguities.

It should be noted that the registration strategy directly utilizing LoD2 models is feasible, with its primary advantage being that it does not require converting the models

into intermediate point clouds, thus making the process concise and efficient. However, a major challenge of this strategy is its dependence on the quantity and quality of features extracted from the models. If the models themselves lack sufficient features, this deficiency can easily result in decreased registration accuracy (Bosché, 2012; Sheik et al., 2022b). To address this issue, an increasing number of researchers are adopting methods that generate 3D point clouds from LoD2 models and convert the original LiDAR-to-Model registration into a typical point cloud registration task.

2.1.2. Registration Using Converted Point Clouds from LoD2 Models

As mentioned in Section 2.1.1, a LiDAR-to-Model registration task can be converted into classic point cloud registration. Over the past few decades, extensive research regarding this topic has been conducted across multiple fields, including geodesy, GIS, computer science, robotics, AEC (Architecture, Engineering, Construction), etc., with each domain emphasizing distinct aspects like scenarios and accuracy. Given that this paper primarily addresses the fine LiDAR-to-Model registration in the context of individual buildings, the following literature review will specifically focus on two relevant categories of registration: ICP-based methods and geometric feature-based methods.

ICP-based methods are extensively employed to register point clouds. Traditional ICP algorithms iteratively align corresponding points but often exhibit slow convergence and sensitivity to initial values and outliers (Besl and McKay, 1992). Thus, many enhanced variants have been developed to address these limitations. For instance, Point-to-Line ICP (Censi, 2008) and Point-to-Plane ICP (Low, 2004; Rusinkiewicz and Levoy, 2001) utilize local linear and planar features, respectively, thereby accelerating convergence and enhancing registration accuracy. Generalized ICP (GICP) further refines registration precision by statistically optimizing correspondences through probabilistic modeling of local surface geometry (Segal et al., 2009). Trimmed ICP (TriICP) effectively reduces the influence of outliers by selectively excluding a certain percentage of correspondences, thereby enhancing robustness in noisy scenarios (Chetverikov et al., 2002). More recently, a robust method based on generated planar patches and adaptive distance thresholds was proposed, which has significantly reduced the influence of surface changes on registration accuracy (Yang and Schwieger, 2023; Yang and Holst, 2025). Collectively, these ICP variants have progressively addressed the limitations in standard ICP, significantly improving the accuracy, efficiency, and practical applicability of point cloud registration tasks.

Compared with the aforementioned ICP-based methods, geometric feature-based methods utilize points, lines, curves, and planes extracted from point clouds to establish correspondences for transformation estimation. These methods are generally less sensitive to variations of initial alignments compared to ICP-based methods. In the building scenarios discussed in this paper, planar features offer notable advantages over other geometric primitives, such as point or line features, and have thus been commonly utilized in point cloud registration tasks (Sheik et al., 2022a; Bosché, 2012; Wujanz et al., 2018; Chen et al., 2019; Xu et al., 2025). This preference arises primarily for two reasons. First, man-made structures typically contain abundant planar elements, naturally facilitating the extraction and use of planar features. Second, planar features demonstrate higher resilience against surface noise and outliers.

More specifically, Scantra (Wujanz et al., 2018), developed by technet GmbH¹, projects the point cloud onto a 2D space and leverages extracted planar information, such as area,

¹<https://www.technet-gmbh.com/en/products/scantra/>

bounding box, boundary length, and average intensity, to establish plane correspondences (Dold and Brenner, 2006). PLADE (Chen et al., 2019) utilizes plane pairs and their spatial intersection lines as structural foundations to construct descriptors, ultimately achieving high-accuracy registration. Both of them are two leading plane-based methods which have been widely used in point cloud registration (Holst et al., 2019; Kaiser et al., 2022; Ma and Wei, 2023).

2.2. Inherent Uncertainty of Models

Compared to the rapid growth in the creation and application of models, research on their uncertainty has lagged behind and not received equivalent attention (Zou and Sester, 2022). Initially, researchers from architecture and archaeology took the lead in visualizing uncertainty associated with models of historical buildings (Zuk et al., 2005; Kensek, 2007). Subsequently, approaches to quantifying uncertainty in models have continued to evolve, with increasingly comprehensive methods proposed, along with the introduction of the concept of Level of Uncertainty (LoU), which systematically characterizes uncertainty variations among different components of building models (Landes et al., 2019; Potter et al., 2012).

With growing demand for high-precision applications relying on semantic 3D city models such as navigation (Kulmer et al., 2025), trajectory estimation (Lucks et al., 2021), and change detection (Meyer et al., 2022), an increasing number of researchers have also begun to investigate the uncertainty inherent in these models (Foschi et al., 2024). For instance, probabilistic methods have been developed for quantifying uncertainty, primarily focusing on semantic labeling in 2D maps or building models (Di et al., 2022; Feng et al., 2021; Paz et al., 2020). Additionally, other researchers have specifically examined the uncertainty associated with facades and windows in semantic 3D city models, quantifying aspects such as their positions and orientations (Zou and Sester, 2022).

Collectively, uncertainty in semantic 3D city models has become increasingly important in high-precision applications, as uncertainty inherent in the model inevitably propagates into downstream use cases. Neglecting these uncertainties or treating the model as an error-free reference is likely to introduce systematic inaccuracies and errors in subsequent processes (Zou and Sester, 2022). Specifically, within the context of accurate building-level LiDAR-to-Model registration discussed in this paper, addressing uncertainty inherent in the model serving as reference data will be a central focus.

3. Methodology

Figure 2 gives an overview of the proposed L2M-Reg. The required inputs are the semantic LoD2 models of the individual building and its corresponding coarsely registered LiDAR point clouds. The LiDAR point clouds could be acquired from MLS systems equipped with GNSS or other well-established coarse registration solutions. The implementation of coarse registration falls outside the scope of this paper, more details can be found from literature (Xu et al., 2017; Bueno et al., 2018; Xu et al., 2019). After pre-processing introduced in Section 3.1, L2M-Reg consists of three key steps: reliable plane correspondence establishment in Section 3.2, pseudo-plane-constrained Gauss–Helmert model in Section 3.3, and adaptable vertical translation estimation in Section 3.4. The core of the L2M-Reg lies in addressing the spatial variation in model uncertainty among different building structural components. L2M-Reg automatically localizes and extracts representative planar regions (i.e., wall plinth) to establish correspondences and obtain 6

DoF transformation parameters. More detailed steps are given in the following subsections.

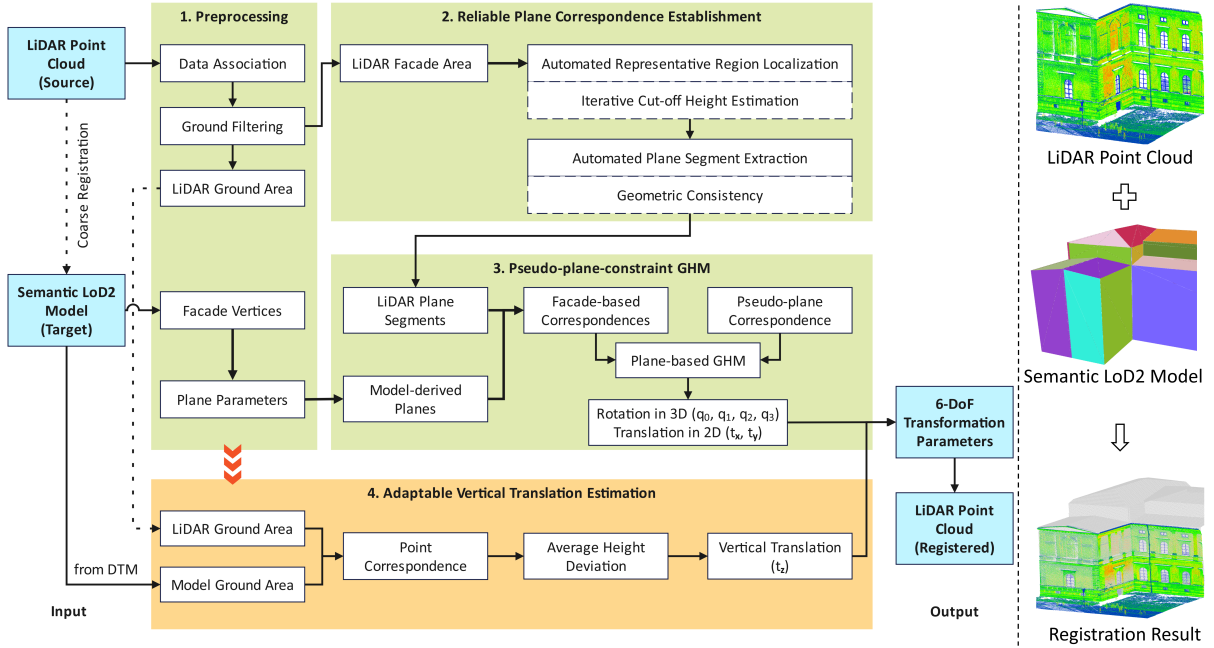


Figure 2: Flowchart of the proposed L2M-Reg. Each plane of the input semantic LoD2 model is colored for better visualization and the point cloud is colored by intensity.

3.1. Data Preprocessing

Data preprocessing is performed on the LiDAR point clouds and corresponding LoD2 models. For outdoor LiDAR-to-Model registration, the required overlapping region between two datasets is generally limited to ground areas and exterior building facades. This is because adopted Terrestrial Laser Scanning (TLS) and Mobile Laser Scanning (MLS) systems cannot capture the roof regions.

Publicly available Digital Terrain Model (DTM) datasets can provide additional ground information, as these datasets are georeferenced and maintained by governmental or professional institutions, ensuring their high authority and accessibility. Consequently, the model information used in this study is primarily from two components: building facades and ground areas adjacent to these facades.

The LoD2 models utilized as reference data comprise multiple wall surfaces with planar geometry representation. Each wall acts as a reference plane for subsequent registration and possesses a unique object ID along with the corresponding coordinates of several vertices, as specified by the CityGML standard. These vertices are employed to calculate the associated plane parameters of each model.

Since the Z-axis of LiDAR point clouds is adjusted to be vertically upward by the sensors, all wall surfaces are assumed to be extruded along their normal vectors in horizontal directions, as shown in Figure 3. The resulting buffer zones with a thickness of 1 m are used to associate individual points with the wall surfaces within whose buffers they reside. The choice of 1 m is mainly based on two considerations: first, many existing LiDAR-to-Model coarse registration methods already achieve decimeter- to centimeter-level accuracy (Diakite and Zlatanova, 2020; Sheik et al., 2022a,b); second, as building

plinths are generally within the centimeter- to decimeter-scale, a 1 m buffer reliably covers them without adding processing overhead. Similarly, the DTM is converted into a triangulated irregular network and extruded to filter out redundant LiDAR data. This process also removes elements such as vegetation and pedestrians located near buildings.

Simultaneously, during the buffer zone-based filtering, each individual point is associated with the corresponding wall surface by assigning them unique wall identifiers, as illustrated in Figure 3. Although the finally usable plane segments are not explicitly extracted at this stage, they must reside within the associated LiDAR point clouds. Accordingly, the correspondence relationships are firmly locked at this step.

In contrast to other plane-based methods that first extract plane segments and then search for correspondences (Sheik et al., 2022a; Wujanz et al., 2018; Chen et al., 2019), this strategy maximizes the utilization of existing semantic information from the models. By reliably fixing correspondence relationships before extracting specific plane segments, this strategy ensures a more effective use of prior information while achieving greater simplicity and efficiency as shown in Section 4.4.3.

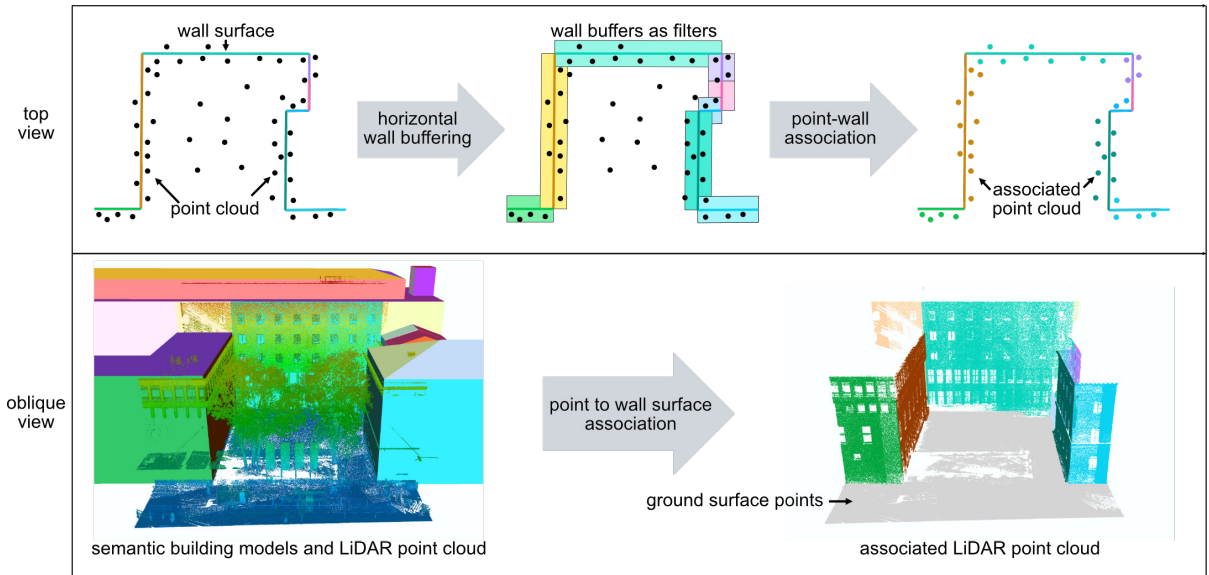


Figure 3: Data association illustration for LiDAR point clouds and wall surfaces. To establish correspondence, only points located within each wall’s buffer zone are retained. The resulting associations are colorized to facilitate clearer interpretation.

The main outputs of data preprocessing consist of the model-derived plane M_i of the facade area and the corresponding neighboring point cloud N_i (equal to the associated LiDAR point clouds shown in Fig 3). The parameters of each M_i are explicitly known, and stable correspondence relationships between N_i and M_i are fixed through data association. In the subsequent step described in Section 3.2, the finally usable plane correspondences will be established.

3.2. Reliable Plane Correspondence Establishment

After data preprocessing, accurately extracting a suited LiDAR plane segment L_i from neighboring point cloud N_i to construct reliable correspondences remains a challenge. To address this, an automated solution is developed, comprising two main parts: representative region localization in Section 3.2.1 and plane segment extraction in Section 3.2.2.

3.2.1. Automated Representative Region Localization

In this part, the input consists of the neighboring point cloud N_i surrounding each model-derived plane M_i , encompassing the full exterior facade area of the building. As noted before, previous plane-based LiDAR-to-Model registration methods often overlook the model uncertainty and directly use the most representative plane from the full neighboring space to establish correspondences. In this case, they implicitly assume that the planes derived from the entire N_i are inherently representative. However, this assumption becomes invalid when considering model uncertainty.

Specifically, in LoD2 models, wall surfaces are typically generated by vertically extruding the building footprint, implying that the model-derived plane M_i should only correspond to the building’s plinth, as shown in Figure 1. This plinth region is actually a subspace of each neighboring point cloud N_i and contains the representative region used for correspondence construction. Therefore, the goal in this step is to automatically localize this representative region. Herein, an iterative cut-off height estimation algorithm is developed to eliminate unsuitable regions and adaptively localize the plinth areas for subsequent LiDAR plane segment L_i extraction. The core of this algorithm lies in the continuous refinement of the neighboring space. As shown in Figure 4, the input neighboring point cloud is N_i , where i denotes the shared ID of the associated model-derived plane M_i . The algorithm is conducted based on the following steps:

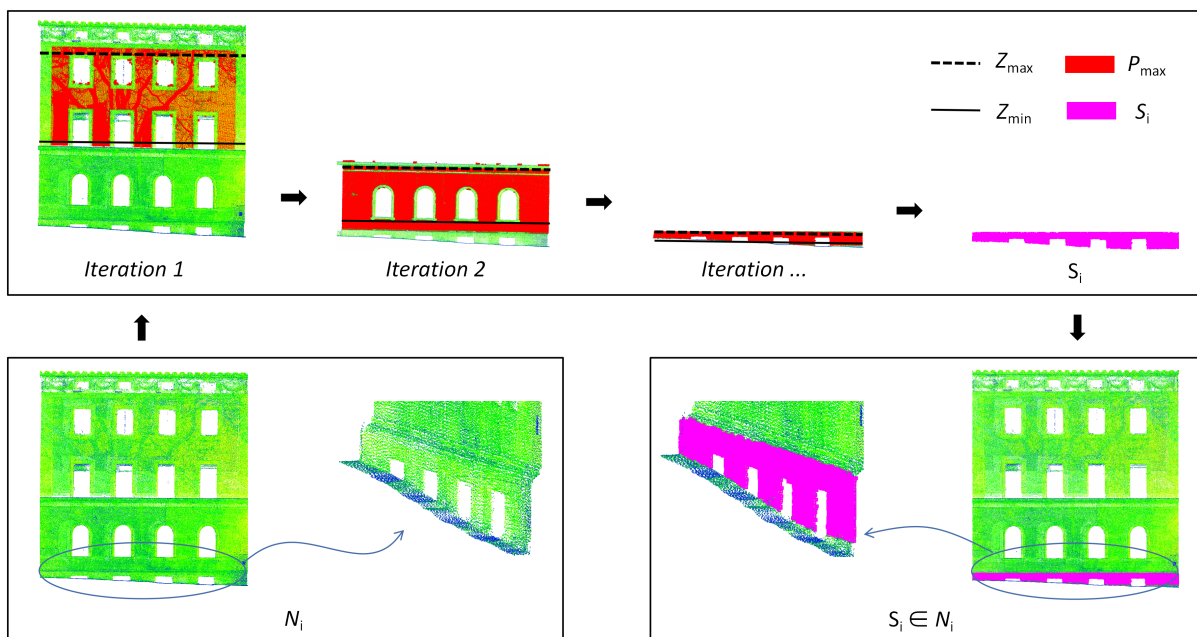


Figure 4: Automated representative region localization. N_i represents the input neighboring point cloud (colored by intensity), and S_i represents the output representative subspace (in purple) corresponding to the building’s plinth.

- (1) Detecting the largest plane from N_i based on Random Sample Consensus (RANSAC) as shown in red part in Fig 4, denoted as P_{\max} . The distance threshold T_{dis} used in the RANSAC is determined based on the registration residual e of the entire input LiDAR point clouds, defined as $T_{dis} = e$. The residual e can be derived from the performance of the multi-station point cloud registration.
- (2) The Z coordinates of all the points in P_{\max} are then sorted in ascending order, and the value at the 10th and 90th percentiles is selected as the lower and upper height

bounds as shown in solid and dashed black lines in Fig 4, respectively, denoted as Z_{\min} and Z_{\max} .

- (3) The angle α between the normal vector of P_{\max} and the ground plane is then calculated. If α exceeds angle threshold T_α , P_{\max} is considered part of the exterior facade. In this case, all points in N_i whose Z coordinates are larger than Z_{\min} are removed, and the P_{\max} extraction process is also recognized as valid. The remaining point cloud is then taken as the updated N_i for the next iteration as shown in Fig 4.

The above steps are repeated until the extraction of P_{\max} is deemed invalid, indicating that all extractable instances of P_{\max} have been traversed from top to bottom along the height direction. The angular threshold T_α is set to a predefined value of 10° , which is empirically determined based on the structural characteristics of typical buildings. The last validly extracted P_{\max} is then selected, and its corresponding Z_{\min} and Z_{\max} values are computed. These values are used to define the final cut-off height range R based on

$$R \in [Z_{\min}, Z_{\max}]. \quad (1)$$

Only the points in N_i whose Z -coordinates fall within this range R are retained, forming the final output representative subspace S_i . The subspace S_i primarily includes the building’s plinth, which serves as the representative region for the subsequent LiDAR plane segment L_i extraction input. The main steps for the iterative cut-off height estimation are shown in Algorithm 1.

Algorithm 1: Iterative Cut-off Height Estimation for Representative Subspace

Input: Neighboring point cloud N_i

Output: Representative subspace S_i

Set angular threshold T_α ;

Set distance threshold T_{dis} ;

repeat

Detect largest plane P_{\max} from N_i using RANSAC with threshold T_{dis} ;

Sort Z coordinates of points in P_{\max} ascendingly ;

Compute $Z_{\min} \leftarrow$ 10th percentile, $Z_{\max} \leftarrow$ 90th percentile ;

Compute angle α between normal of P_{\max} and ground plane ;

if $\alpha > T_\alpha$ **then**

Remove all points in N_i where $Z > Z_{\min}$;

Update N_i with remaining points ;

Mark extraction as valid ;

else

Mark extraction as invalid ;

until extraction of P_{\max} is invalid;

Let last valid P_{\max} define Z_{\min}, Z_{\max} ;

Define cut-off height range $R \leftarrow [Z_{\min}, Z_{\max}]$;

Retain points in N_i where $Z \in R$ to form final subspace S_i ;

return S_i

3.2.2. Automated Plane Segment Extraction

After obtaining the subspace S_i from N_i , the next task is to extract the desired LiDAR plane segment L_i from S_i to establish a correspondence with M_i . It is worth noting that the actual point cloud of N_i is often incomplete due to occlusions caused by vegetation, vehicles, pedestrians, and other objects during data acquisition. Additionally, the facades and plinths of some buildings may be relatively rough and contain various irregular microstructure elements. Under such conditions, direct plane extraction typically results in a large number of discrete planes oriented in different directions.

The desired LiDAR plane segment L_i should be as representative as possible and accurately reflect the location of the building's footprint. To accomplish this, an automated extraction algorithm is developed, with the main steps outlined as follows:

- (1) Plane extraction is performed on the S_i using RANSAC, with the same distance threshold T_{dis} defined previously. For each extracted plane, the angle between its normal vector and the ground plane is calculated. Only those planes with angles exceeding T_α are retained as candidate planes.
- (2) The candidate planes are then clustered based on the similarity of their normal vectors, using a stricter angular threshold defined as $T_\theta = 0.5T_\alpha$ to further group geometrically similar planes. Subsequently, the planes within each cluster are merged to form unified planar regions.
- (3) The largest merged plane is selected as the initial seed plane and then gradually extended by incorporating candidate points from other merged planes that exhibit geometric consistency (GC). To formally define GC, let the current seed plane be denoted by ω_0 , expressed in the general form:

$$\omega_0 : \mathbf{n}_0 \cdot \mathbf{x} + d_0 = 0 \quad (2)$$

where $\mathbf{n}_0 \in \mathbb{R}^3$ is the unit normal vector of the seed plane, $d_0 \in \mathbb{R}$ is the offset term, and $\mathbf{x} \in \mathbb{R}^3$ represents a point in 3D space. Given a candidate point $\mathbf{p} = (x_p, y_p, z_p)^T$, its perpendicular distance to the seed plane is computed as:

$$d(\mathbf{p}, \omega_0) = |\mathbf{n}_0 \cdot \mathbf{p} + d_0|. \quad (3)$$

If \mathbf{p} is temporarily added and a new plane is re-estimated, let \mathbf{n}_{new} denote the updated unit normal vector. The angular deviation between the original and updated planes is then given by:

$$\theta = \arccos(\mathbf{n}_0 \cdot \mathbf{n}_{new}). \quad (4)$$

A candidate point \mathbf{p} is accepted by ω_0 if both the distance and angular consistency criteria are satisfied:

$$GC(\mathbf{p}, \omega_0) = \begin{cases} \text{true,} & \text{if } d(\mathbf{p}, \omega_0) < T_{dis} \text{ and } \theta < T_\theta \\ \text{false,} & \text{otherwise.} \end{cases} \quad (5)$$

- (4) The extended plane obtained in step (3) is used as the final candidate point set. The plane is then re-fitted to this set using least-squares, and points within the T_{dis} are retained as the desired LiDAR plane segment L_i , effectively eliminating residual noise.

More details are shown in Algorithm 2. The proposed plane extraction algorithm is better suited than the classic RANSAC to extract representative planes from irregular and rough areas in real-world scenarios. Typically, RANSAC identifies a set of inliers that satisfy predefined threshold. It outputs the plane corresponding to the largest inlier set while discarding all outliers by default.

Algorithm 2: Automated Plane Segment Extraction

Input: Reliable subspace S_i, T_{dis}, T_α
Output: Desired LiDAR plane segment L_i
Initialize candidate plane set $\mathcal{P} \leftarrow \emptyset$;
Perform RANSAC-based plane extraction on S_i ;
foreach *extracted plane* P **do**
 Compute angle α between normal of P and ground plane ;
 if $\alpha > T_\alpha$ **then**
 Add P to \mathcal{P} ;
Cluster planes in \mathcal{P} based on normal vector similarity using $T_\theta \leftarrow 0.5T_\alpha$;
Merge planes within each cluster into unified planar regions ;
Select the largest merged plane as seed plane ω_0 with normal \mathbf{n}_0 and offset d_0 ;
Initialize point set $Q \leftarrow$ points in ω_0 ;
foreach *candidate point* \mathbf{p} *from other merged planes* **do**
 Compute point-to-plane distance $d(\mathbf{p}, \omega_0)$ using Eq. (3) ;
 Temporarily add \mathbf{p} to Q and re-estimate plane ω_{new} with normal \mathbf{n}_{new} ;
 Compute angular deviation θ using Eq. (4) ;
 if $d(\mathbf{p}, \omega_0) < T_{dis}$ **and** $\theta < T_\theta$ **then**
 Accept \mathbf{p} into Q based on geometric consistency (Eq. (5)) ;
 Update ω_0 with new estimate ;
Refit plane to Q using least-squares ;
Retain all points in Q within distance T_{dis} to obtain final LiDAR plane segment L_i ;
return L_i

However, in practice, the building surface may contain many small-scale irregularities or exhibit pronounced roughness. In addition, due to registration residual introduced by multi-station scanning, the input point clouds used for plane extraction may suffer from local layer separation. In such cases, some of the points rejected by RANSAC as outliers may, in fact, still be suited and usable. By leveraging GC check as shown in Fig 5, the proposed algorithm supplements the inlier set with structurally coherent points from other sets and outliers. This enhances the representativeness of the final extracted plane while preserving the overall consistency of extraction quality.

After the above process is completed, the output is the final LiDAR plane segment L_i , whose corresponding model-derived plane M_i has already been fixed during preprocessing. However, it is important to note that all current plane correspondences only cover building exterior facade or plinth area. To achieve the 6 DoF parameter estimation, additional correspondence from the ground area is still required. This issue will be addressed in the following Section 3.3.

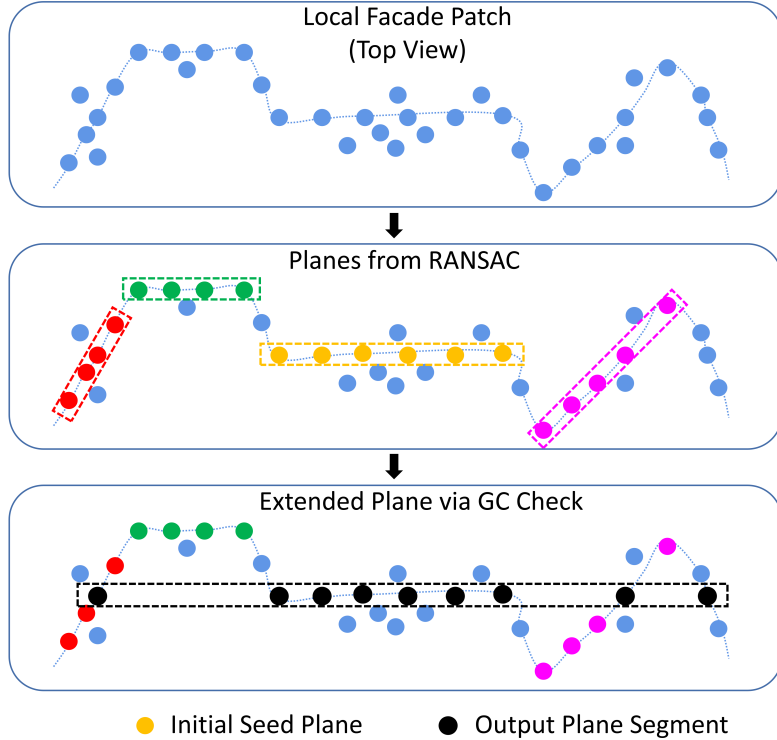


Figure 5: Desired LiDAR plane segment extraction based on geometric consistency (GC) from local facade patch. Blue points indicate a rough facade patch at a local scale. Distinct planes extracted and merged using RANSAC are shown in different colors, while black highlights the plane segments extended after the GC check, representing more complete and representative structures.

3.3. Pseudo-plane-constraint Gauss–Helmert Model

Through previous steps, all facade-based correspondences are available. However, ground-plane correspondences are still missing. Unlike facade areas that typically offer sufficient geometric information through well-defined vertical structures, ground areas are often underrepresented in LoD2 models. The commonly used strategy is to extract ground planes directly from publicly available DTM data, which are then combined with facade-based correspondences to jointly estimate the full transformation (Kumar et al., 2019; Schuegraf et al., 2024). This strategy assumes that DTM data accurately represent the true ground surface and can reliably constrain vertical translation.

However, in practice, the effectiveness of DTM data is often limited. Most DTM data are derived from Airborne Laser Scanning (ALS), which provides significantly lower resolution and geometric accuracy than the TLS or MLS data used for facade-based correspondences (Macay Moreira et al., 2013), as shown in Figure 6. As a result, the relatively low vertical accuracy of DTM-derived correspondences will introduce uncertainty into the overall transformation estimation. In particular, errors in the vertical direction may propagate and adversely affect the estimation of other components, such as horizontal translation and rotation, ultimately compromising the accuracy and stability of the full parameter estimation. This is primarily due to the coupled nature of estimation using plane-based Gauss–Helmert Model (GHM), where vertical inaccuracies can distort the orientation of fitted planes and bias the least-squares optimization process, thereby contaminating the estimation of parameters in other directions.

To address this, a decoupled 2D–3D estimation strategy is proposed to effectively prevent vertical inaccuracies from propagating into other components. Specifically, a

pseudo-plane correspondence is introduced to replace the unreliable correspondence from DTM and provide additional constraint in the GHM adjustment.

The pseudo-plane correspondence consists of two planes with identical normal vectors, simulating the ground surfaces in the target models and the source LiDAR point clouds, respectively. Both planes are defined as:

$$\omega_{\text{target}} : \quad \mathbf{n} \cdot \mathbf{x} + d_t = 0 \quad (6)$$

$$\omega_{\text{source}} : \quad \mathbf{n} \cdot \mathbf{x} + d_s = 0 \quad (7)$$

where \mathbf{n} is a fixed unit normal vector $\mathbf{n} = [0, 0, 1]$ pointing vertically upward. The offset terms are also set to be equal, i.e., $d_t = d_s = 0$, such that the pseudo-planes are fully coincident in space. As seen in Figure 6, this design ensures that the pseudo-plane correspondence introduces no actual height difference and serves solely as a formal constraint to stabilize the vertical component of the transformation during estimation.

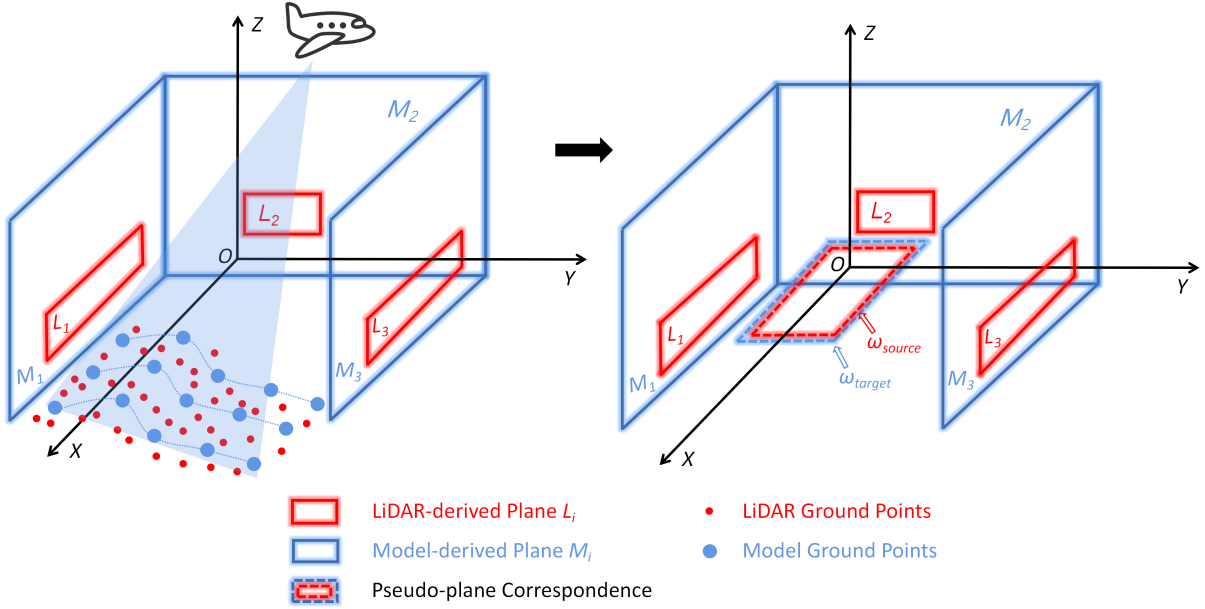


Figure 6: Introduced pseudo-plane correspondence. L_i and M_i denote the LiDAR-derived and model-derived planes, respectively, and serve as facade-based correspondences for registration. The dashed lines represent the introduced pseudo-plane correspondence, which serve as substitutes for the original constraints derived from the LiDAR ground points and model ground points (DTM), indicated by red and blue round dots, respectively.

In the classic plane-based GHM, each plane correspondence contributes a constraint of the form:

$$f = \mathbf{n}_i(\mathbf{R}\mathbf{x} + \mathbf{t}) + d_i = 0 \quad (8)$$

where \mathbf{n}_i and d_i denotes the normal vector and offset term of the model-derived plane M_i , \mathbf{x} is a point on the LiDAR plane segment L_i , $\mathbf{R} \in \mathbb{R}^{3 \times 3}$ and $\mathbf{t} = [t_x, t_y, t_z]^T$ are the rotation matrix and translation vector to be estimated, respectively.

To ensure numerical stability and avoid gimbal lock, rotation is represented using a unit quaternion $\mathbf{q} = [q_0, q_1, q_2, q_3]^T$ with $\|\mathbf{q}\| = 1$. The unknown parameter vector is defined as:

$$\mathbf{X} = [q_0, q_1, q_2, q_3, t_x, t_y, t_z]^T. \quad (9)$$

The classic constraint GHM is already well-established (Mikhail and Ackermann, 1976; Holst et al., 2014; Kalenjuk and Lienhart, 2022). Here, the original constraint is from quaternions, as seen in Eq.(10). Three Jacobian matrices of the constraint GHM are calculated as shown in Eq.(11):

$$c = \sqrt{q_0^2 + q_1^2 + q_2^2 + q_3^2} = 1 \quad (10)$$

$$\mathbf{A}_{[n \times 7]} = \left. \frac{\partial f}{\partial \mathbf{X}} \right|_{\mathbf{x}_0, \mathbf{V}_0} \quad \mathbf{B}_{[n \times 3n]} = \left. \frac{\partial f}{\partial \mathbf{V}} \right|_{\mathbf{x}_0, \mathbf{V}_0} \quad \mathbf{C}_{[1 \times 7]} = \left. \frac{\partial c}{\partial \mathbf{X}} \right|_{\mathbf{x}_0} \quad (11)$$

n is the number of observations and \mathbf{V} is the correction of observations. \mathbf{C} is the matrix composed of the derivatives of the constraint c concerning \mathbf{X} . It is worth noting that when only facade-based correspondences are available, the structure of the matrix \mathbf{A} takes the following form:

$$\mathbf{A}_{\text{facade only}} = \frac{\partial f}{\partial \mathbf{X}} = \begin{bmatrix} \frac{\partial f_1}{\partial q_0} & \frac{\partial f_1}{\partial q_1} & \frac{\partial f_1}{\partial q_2} & \frac{\partial f_1}{\partial q_3} & \frac{\partial f_1}{\partial t_x} & \frac{\partial f_1}{\partial t_y} & 0 \\ \frac{\partial f_2}{\partial q_0} & \frac{\partial f_2}{\partial q_1} & \frac{\partial f_2}{\partial q_2} & \frac{\partial f_2}{\partial q_3} & \frac{\partial f_2}{\partial t_x} & \frac{\partial f_2}{\partial t_y} & 0 \\ \vdots & \vdots & \vdots & \vdots & \vdots & \vdots & \vdots \end{bmatrix}. \quad (12)$$

Due to the absence of ground-plane constraints, the rightmost column of \mathbf{A} , corresponding to the vertical translation t_z , consists entirely of zeros, resulting in a rank-deficient system in the vertical direction. This may result in an unsolvable or invalid solution.

The incorporation of the pseudo-plane correspondence introduces an additional ground-plane constraint. As two pseudo-planes are deliberately constructed with identical parameters and perfectly aligned geometry, this data-driven constraint introduces no residual, but provides an additional condition that reinforces the existing GHM system. The structure of the new matrix \mathbf{A} is converted to the following form:

$$\mathbf{A}_{\text{with pseudo-plane}} = \frac{\partial f}{\partial \mathbf{X}} = \begin{bmatrix} \frac{\partial f_1}{\partial q_0} & \frac{\partial f_1}{\partial q_1} & \frac{\partial f_1}{\partial q_2} & \frac{\partial f_1}{\partial q_3} & \frac{\partial f_1}{\partial t_x} & \frac{\partial f_1}{\partial t_y} & 0 \\ \frac{\partial f_2}{\partial q_0} & \frac{\partial f_2}{\partial q_1} & \frac{\partial f_2}{\partial q_2} & \frac{\partial f_2}{\partial q_3} & \frac{\partial f_2}{\partial t_x} & \frac{\partial f_2}{\partial t_y} & 0 \\ \vdots & \vdots & \vdots & \vdots & \vdots & \vdots & \vdots \\ 0 & 0 & 0 & 0 & 0 & 0 & 1 \end{bmatrix}. \quad (13)$$

As a result, 3D rotation and horizontal translation (t_x and t_y) can be accurately estimated, because the t_z currently obtained is always zero or very close to zero. The actual vertical translation t_z will be solved separately in the following Section 3.4.

The primary advantage of this strategy lies in its ability to perform reliable parameter estimation even in the absence of real ground-plane correspondences. More importantly, it effectively decouples the influence of low-quality observations—such as those derived from DTM data—from high-quality observations, preventing error propagation across components and maximizing the use of reliable facade-based correspondences.

On the one hand, such design remains adaptable to ground data of varying types, accuracies, and acquisition sources. This adaptability becomes even more evident in scenarios with sloped or uneven ground surfaces, where simply constraining or omitting the parameter in a given direction—such as t_z in the GHM—may still introduce additional

errors. On the other hand, rather than omitting the estimation of t_z and solving only for five parameters, the pseudo-plane strategy offers greater flexibility and adaptability, making it readily extendable to other facade orientations. Overall, the pseudo-plane strategy delivers a balanced design that preserves estimation robustness while maintaining adaptability to diverse scenarios.

3.4. Adaptable Vertical Translation Estimation

In this step, the goal is to estimate the remaining vertical translation t_z . The transformation parameters obtained from the previous step are first applied to the LiDAR point clouds to achieve alignment in all directions except the vertical axis. Next, DTM data is utilized to establish point correspondences. Specifically, after denoising the transformed ground point clouds, each DTM point is used as a reference center, and its nearest neighbors within a certain radius in the XOY plane are searched in the point clouds. As seen in Figure 7, these local neighbors are then used to construct a set of vertical correspondences. The average deviation in the Z-coordinates across all correspondences is computed to obtain the final estimate of the vertical translation t_z .

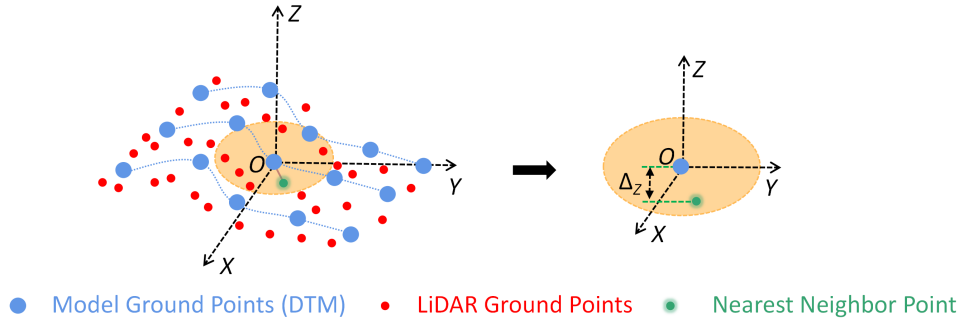


Figure 7: Vertical translation estimation

In this way, the vertical translation t_z can be easily estimated from DTM data while preserving a high degree of flexibility, benefiting from the aforementioned 2D–3D decoupled estimation strategy. For instance, if more accurate vertical information becomes available—such as GNSS observations, total station measurements, or other high-fidelity ground models—the DTM can be seamlessly substituted using the same method. This design greatly enhances the adaptability of the overall framework to heterogeneous data sources and ensures robustness under varying data availability conditions.

4. Experiment and Results

This part introduces the experiment and results, including data preparation in Section 4.1, experiment design in Section 4.2, evaluation metrics in Section 4.3, and comparison results in Section 4.4.

4.1. Data Preparation

To validate and evaluate the proposed L2M-Reg, three datasets (as shown in Figure 8), named as TUM0501 Building, Pinakothek, and Street Building, are collected, comprising LiDAR point clouds of buildings based on TLS or MLS from the urban areas of Munich. Besides, the corresponding publicly accessible LoD2 models are obtained

from the Bavarian Surveying Administration². These datasets vary in point cloud size, building size, and data acquisition methods.

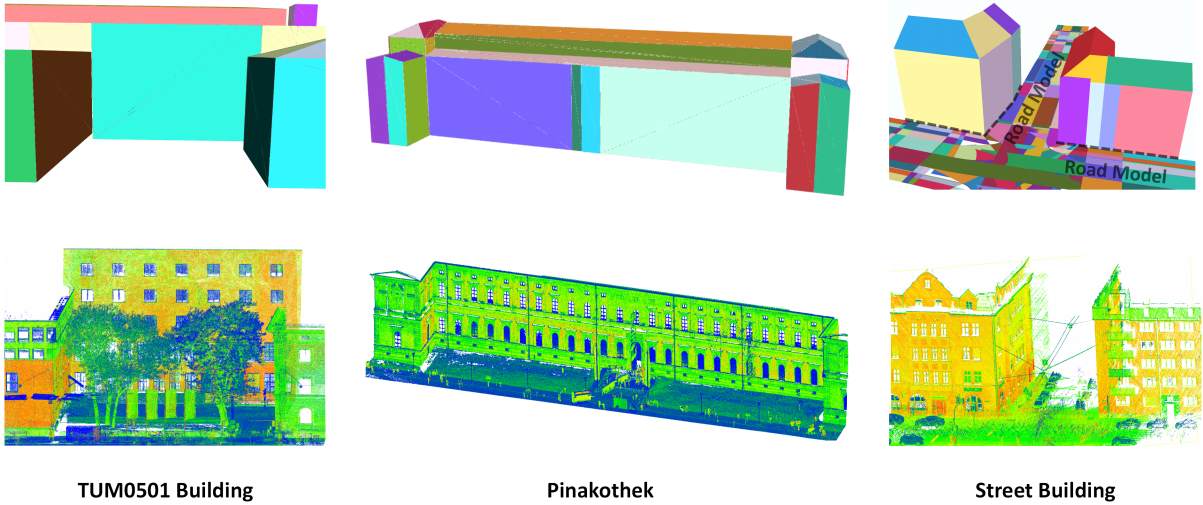


Figure 8: Overview of three datasets. The upper part shows the LoD2 semantic models, with planes colored for visual distinction. The lower part displays the corresponding point clouds, colored by intensity.

In particular, due to the absence of ground data in the publicly accessible LoD2 models, ground information for the TUM0501 Building and Pinakothek datasets which are part of the TUM2TWIN³ (Wysocki et al., 2025) is supplemented by publicly available DTM data with a grid width of 1 m from the Bavarian Surveying Administration. The Street Building dataset utilizes an additional georeferenced road model. Further details of the datasets are summarized in Table 1.

	TUM0501 Building	Pinakothek	Street Building
Number of Points	2,272,810	10,367,229	5,000,509
Scanning Area	About 1,200 m ²	About 36,000 m ²	About 1,500 m ²
Scanning System	Leica ScanStation P50	Leica ScanStation P50	Z+F FlexScan 22
Scanning Technique	TLS	TLS	MLS
Ground Data Source	DTM	DTM	Road Model

4.2. Experiment Design

In addition to the proposed L2M-Reg, four existing methods — GICP (Segal et al., 2009), TriICP (Chetverikov et al., 2002), PLADE (Chen et al., 2019) and Scantra (Wujanz et al., 2018) — are also applied to the three datasets for performance evaluation and comparison. GICP and TriICP are chosen as leading robust ICP-variants, known for their reliability in fine-registration tasks. PLADE and Scantra are included as the two leading plane-based registration methods. Since these registration methods are inherently designed for point clouds rather than parametric models, the LoD2 models from the three datasets were converted into point clouds with uniform density to facilitate registration using the four methods mentioned above.

²<https://geodaten.bayern.de/opengeodata/>

³<https://tum2t.win/>

L2M-Reg was implemented in C++ using Point Cloud Library (PCL) (Rusu and Cousins, 2011). Standard implementations of GICP and TriICP in PCL (version 1.13.0) were utilized, while PLADE was implemented based on its open-source release⁴ (Chen et al., 2019). Scantra was tested on the basis of the latest version 3.4 released in 2025⁵. All methods were executed under identical hardware conditions (Intel Xeon(R) W-2223 CPU@3.60GHz with 4 Cores and 64 GB of RAM).

4.3. Evaluation Metrics

To quantitatively evaluate the registration accuracy, the M3C2 distance (Lague et al., 2013) between the registered LiDAR point clouds and the reference model is computed. Subsequently, a set of check points p is uniformly selected from stable regions near building footprints, extending in various directions within each scene, to assess horizontal ($p \in H_i$) and vertical ($p \in V_i$) registration error. The average horizontal error Err_H and vertical error Err_V are defined by the average M3C2 distance at all check points, as calculated by

$$Err_H = \frac{1}{n_H} \sum_{p \in H_i} \delta_{M3C2}(p), \quad (14)$$

$$Err_V = \frac{1}{n_V} \sum_{p \in V_i} \delta_{M3C2}(p), \quad (15)$$

where n_H and n_V denote the number of check points used for assessing horizontal and vertical error, respectively. For each check point p , $\delta_{M3C2}(p)$ represents the M3C2 distance between p and the reference model. Similarly, based on Equation 14 and Equation 15, the standard deviation of M3C2 distances in the horizontal and vertical directions can be computed by

$$Std_H = \sqrt{\frac{1}{n_H - 1} \sum_{p \in H_i} (\delta_{M3C2}(p) - Err_H)^2}, \quad (16)$$

$$Std_V = \sqrt{\frac{1}{n_V - 1} \sum_{p \in V_i} (\delta_{M3C2}(p) - Err_V)^2}. \quad (17)$$

These evaluation metrics are used for two primary reasons. First, the M3C2 distance is more robust to noise and non-uniform point spacing than the nearest Cloud-to-Cloud (C2C) distance, providing a more accurate measure of geometric consistency between point clouds and models. Second, sampling from geometrically stable regions (i.e., footprint area) in both horizontal and vertical directions reduces the influence of dynamic elements such as vegetation and pedestrians, thus improving the reliability of the accuracy assessment.

⁴<https://github.com/chsl/PLADE>

⁵<https://www.technet-gmbh.com/en/products/scantra/scantra-news/scantra-release-34-static-kinematic-and-polar-are-ready-for-download/>

4.4. Comparison Results

The following part systematically demonstrates the performance of L2M-Reg in terms of accuracy and efficiency through qualitative comparison in Section 4.4.1, quantitative comparison in Section 4.4.2, and efficiency analysis in Section 4.4.3.

It is important to note that, unlike conventional evaluations based on the overall geometric closeness of the entire building, this study — motivated by the focus on model uncertainty — adopts the building footprint area as the primary basis for evaluation. This choice stems from the fact that, during LoD2 model generation, the near-ground footprint area is typically the most suited and accurately reflects the building’s true location, especially when there is a horizontal offset between plinth and facade. Accordingly, all subsequent evaluations in this study assess horizontal accuracy merely based on the distance between the aligned LiDAR point clouds and LoD2 models in the footprint area.

4.4.1. Qualitative Comparison

Figures 9, 10 and 11 present the valid registration results in three datasets. During testing, TriICP, GICP, and L2M-Reg consistently produced valid results, whereas PLADE failed to do so for the TUM0501 Building dataset. Scantra also exhibited suboptimal performance across three datasets. Possible reasons for these shortcomings are discussed in Section 5.

As shown in Figure 9, the TUM0501 Building dataset yields valid registration results using TriICP, GICP, and L2M-Reg. The results of PLADE and Scantra are not included, as neither produces valid results in this case. In the horizontal direction, particularly within the building footprint areas outlined by dashed circles, L2M-Reg achieves the highest consistency compared to TriICP and GICP. In the vertical direction, it also shows superior alignment with the ground model, further highlighting its advantage in registration accuracy.

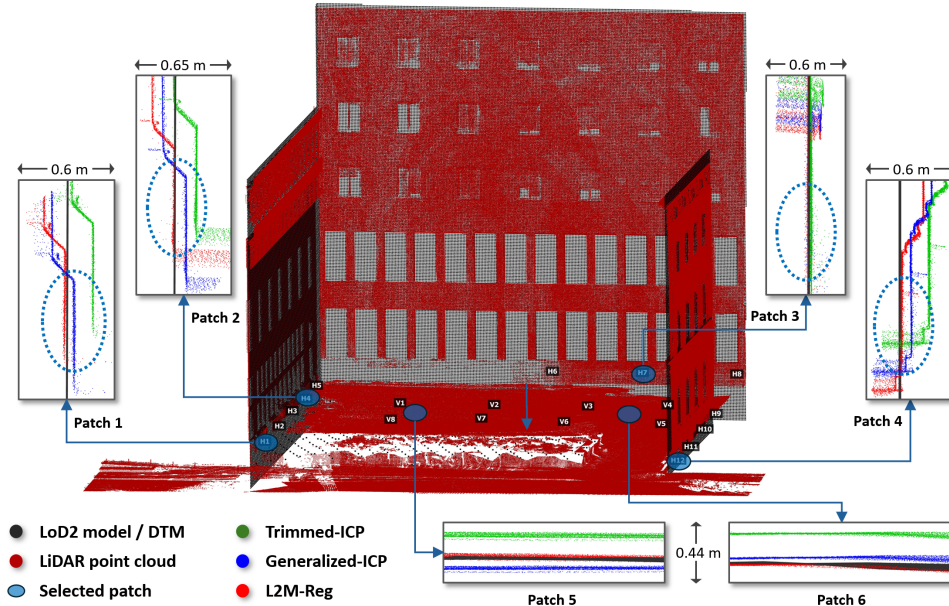


Figure 9: Registration performance of different methods in the TUM0501 dataset

Figure 10 shows all valid registration results for the Pinakothek dataset. In the horizontal direction, L2M-Reg consistently demonstrates higher accuracy within the footprint area, as illustrated in Patch 1 to Patch 5 (outlined by dashed circles). Notably, in Patch

6, L2M-Reg exhibits a visible deviation from the reference model compared to the two ICP-based methods. This discrepancy is primarily attributed to scale inaccuracies in the LoD2 model, resulting in dimensional mismatches between the model and the point cloud. Despite this, L2M-Reg still achieves the globally optimal registration, as evidenced by Patch 1 being parallel to Patch 6, where L2M-Reg again provides a better global fit. In the vertical direction, as shown in Patch 7 to Patch 9, L2M-Reg demonstrates the best alignment between point clouds and DTM.

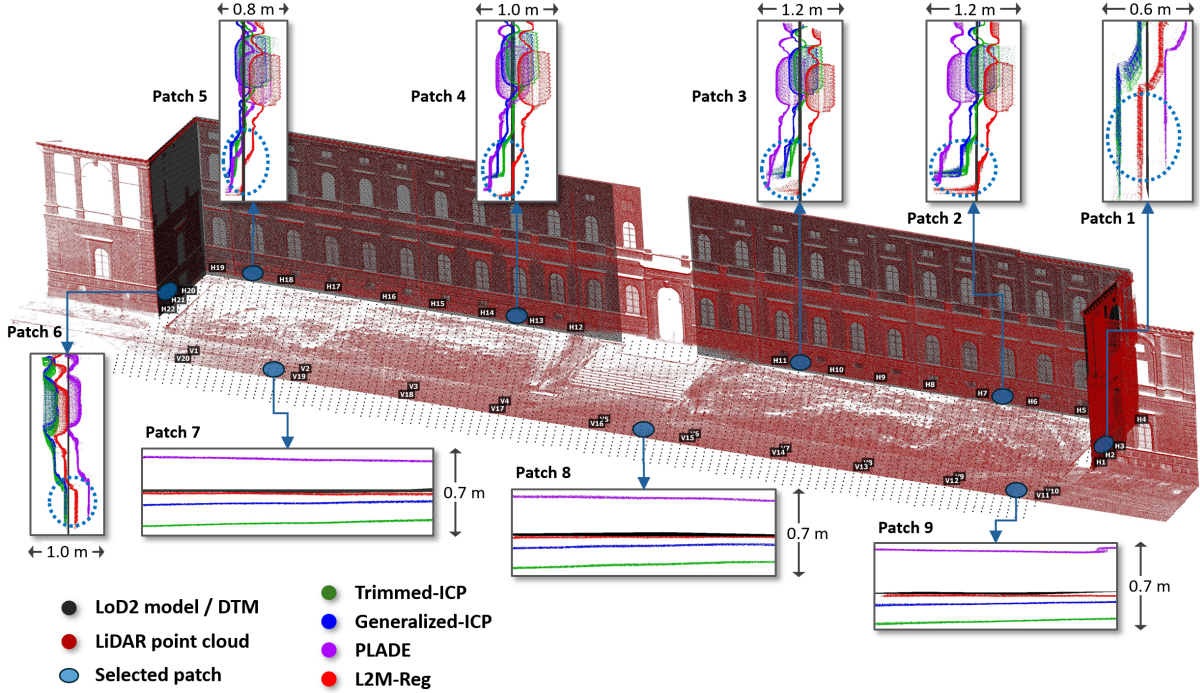


Figure 10: Registration performance of different methods in the Pinakotheek Dataset

In the Street Building dataset, shown in Figure 11, L2M-Reg consistently delivers the most accurate alignment in the horizontal direction, particularly in Patch 1 and Patch 4. The similar slight dimensional mismatches between the models and the point clouds are observed in Patch 2 and Patch 3, as seen in the Pinakotheek dataset. These mismatches are again attributed to scale inaccuracies introduced in the original models. Nevertheless, L2M-Reg achieves a globally optimal result, with the registered point clouds (in red) centrally aligned between the two corresponding facades of the LoD2 models in Patch 2 and Patch 3.

In the vertical direction (e.g., Patch 6), L2M-Reg achieves the best alignment with the reference model in most regions. However, in certain areas like Patch 5, it does not produce optimal results. This results from the road being originally described according to the OpenDRIVE standard (ASAM, 2024; Kutsch et al., 2024), which models individual lanes with overlapping surface geometries and continuous curvature. The parametric surface representations are then sampled to explicit planar surface geometries as part of the conversion to CityGML 3.0 (Schwab et al., 2020). Although unintended overlapping surface geometries introduce minor instability in the evaluation of vertical accuracy, this demonstrates that L2M-Reg can also directly incorporate further object classes of the model, such as the road surface, into the vertical alignment process. Since CityGML 3.0 enables a comprehensive and redundancy-free representation of the road space, such ambiguities are not introduced in native mapping processes.

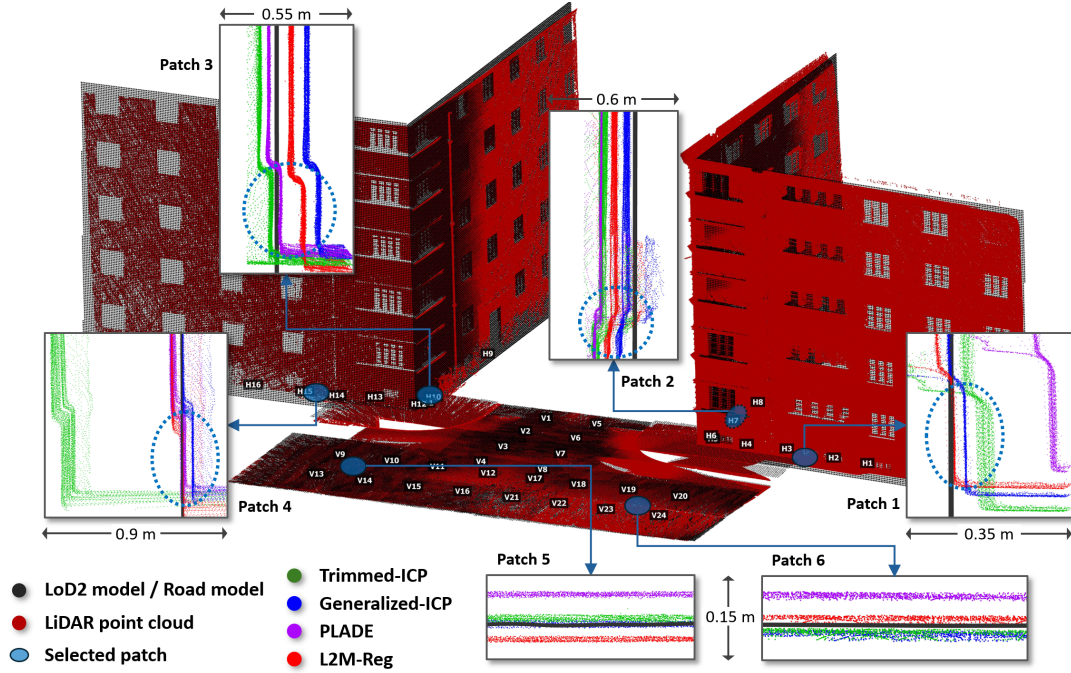


Figure 11: Registration performance of different methods in the Street Building dataset. Patches 1 to 4 correspond to the registration results of the four facades from right to left. Due to viewpoint occlusion, Patch 2 is located on the second facade from the right.

In general, the qualitative comparison results indicate that L2M-Reg outperforms the other methods in both horizontal and vertical consistency in the three datasets. More detailed quantitative evaluation results are presented in Section 4.4.2.

4.4.2. Quantitative Comparison

In this section, the aforementioned evaluation metrics are used to quantitatively compare the four valid registration methods (TriICP, GICP, PLADE, and L2M-Reg) based on the check points manually selected from stable areas. Table 2 shows the number of check points used in each dataset. In the Street Building dataset, all ground points in the central areas of the road were used for vertical error evaluation, considering local layering issues in the road model.

Table 2: The Number of Check Points Used in Three Datasets

	TUM0501 Building	Pinakothek	Street Building
Horizontal check points	12	22	16
Vertical check points	8	20	620

Table 3 reports the average registration error in both horizontal and vertical directions. L2M-Reg achieves the best performance on all three datasets, which is consistent with the qualitative results discussed before. The sole exception lies in the vertical error of the Street Building dataset, where L2M-Reg (2.30 cm) performs slightly worse than GICP (1.89 cm). This minor discrepancy is primarily attributed to the reference ground data, which is derived from an additional road model rather than a standard DTM. Minor layering artifacts in this road model introduce local inconsistencies that bias the vertical error calculation. Nevertheless, the resulting loss (less than 0.5 cm) is negligible for most practical purposes.

Table 3: Average Error Comparison on Three Datasets (cm)

		TriICP	GICP	PLADE	L2M-Reg (Ours)
TUM0501	Err_H	14.07	5.75	–	0.98
	Err_V	24.44	6.24	–	1.20
Pinakothek	Err_H	12.23	18.13	32.36	3.01
	Err_V	24.86	9.20	31.13	2.03
Street Building	Err_H	24.31	6.68	11.77	4.87
	Err_V	2.89	1.89	6.71	2.30

Note: “–” indicates that the method failed to produce valid results; Bold values indicate the best performance.

Table 4 presents the standard deviation of the M3C2 distance across all check points. L2M-Reg consistently achieves the lowest standard deviation across all three datasets, indicating its effectiveness in producing globally optimal and stable registration results. A similar issue can be observed again in the vertical direction of the Street Building dataset. As previously noted, this slight inconsistency primarily stems from the characteristics of the road model. Given the magnitude of the difference, the deviation remains within a negligible range.

Table 4: Standard Deviation Comparison on Three Datasets (cm)

		TriICP	GICP	PLADE	L2M-Reg (Ours)
TUM0501	Std_H	7.46	3.39	–	0.81
	Std_V	3.24	3.71	–	0.72
Pinakothek	Std_H	5.15	6.83	17.09	3.91
	Std_V	2.22	1.32	4.16	0.72
Street Building	Std_H	22.3	6.06	9.99	6.05
	Std_V	2.19	1.37	3.28	1.50

Note: “–” indicates that the method failed to produce valid results; Bold values indicate the best performance.

In summary, both qualitative and quantitative comparisons demonstrate that L2M-Reg achieves superior performance on both the TUM0501 and Pinakothek datasets, as reflected in lower average error and standard deviations. For the Street Building dataset, L2M-Reg also outperforms other methods in horizontal error. Although it does not exhibit a clear advantage in vertical error for this dataset, its performance remains fully comparable to that of the best-performing method (GICP). Overall, the results prove the effectiveness of L2M-Reg and highlight its leading performance across diverse building scenarios.

4.4.3. Efficiency Analysis

Table 5 summarizes the running times of L2M-Reg in comparison to GICP, TriICP and PLADE on three datasets. All methods are evaluated under identical hardware conditions, with a maximum iteration limit of 100. Scantra is excluded from this comparison as it failed to yield valid results.

The results in Table 5 demonstrate that L2M-Reg exhibits promising computational efficiency, particularly on the Pinakothek and Street Building datasets, which contain larger numbers of points. The primary reason is that both ICP-based method and PLADE operate on the entire point clouds, leading to computational times scaling linearly with the number of points. In contrast, L2M-Reg significantly reduces the computing time by

first fixing correspondence relationships within data association and selectively processing points from building plinth. Moreover, as a plane-based method, its complexity is less sensitive to point density, leading to notable improvements in runtime performance.

Table 5: Comparison of Computational Efficiency (Bold values indicate the best performance)

	TUM0501 Building	Pinakothek	Street Building
GICP	30.4s	329.5s	328.6s
TriICP	38.5s	356.1s	120.2s
PLADE	81.2s	182.4s	140.9s
L2M-Reg (Ours)	38.0s	135.9s	52.7s

5. Discussion

This part further discusses the advantages of L2M-Reg in Section 5.1, comparison among three plane-based methods in Section 5.2, reasons of using road model in the Street Building Dataset in Section 5.3, and limitations of L2M-Reg in Section 5.4, providing a deeper understanding of its performance and applicability.

5.1. Advantages of Using Existing Model Semantics and Pseudo-plane Constraint

Compared to existing ICP-based (e.g., GICP and TriICP) and plane-based (e.g., PLADE and Scantra) registration methods that exclusively process point clouds generated from LoD2 models, L2M-Reg uniquely leverages built-in semantic information in LoD2 models. Using these semantic attributes and distinct plane identifiers, facade elements can be efficiently and accurately extracted, enabling precise plane correspondence establishment. This strategy bypasses the conventional two-step workflow of feature extraction followed by correspondence matching. Instead, it directly streamlines correspondence identification by leveraging the existing semantic information in LoD2 models, thus improving the registration robustness and efficiency.

As one of the key innovations of L2M-Reg, introducing the pseudo-plane constraint offers three distinct advantages. First, it enables 2D–3D decoupled parameter estimation, effectively preventing low-quality elevation data from influencing the estimation of other parameters. Second, it is formulated within a clear and interpretable mathematical framework under the GHM and can be implemented with minimal complexity. Third, compared to the alternative of manually fixing t_z to zero in GHM to isolate vertical errors, the pseudo-plane strategy provides greater flexibility and adaptability, allowing for extension to other facade orientations. Moreover, in scenarios involving sloped or uneven ground surfaces, directly constraining t_z in GHM may introduce additional errors, further highlighting the advantages of the pseudo-plane strategy.

5.2. Interpretation of Performance Differences among Three Plane-based Methods

As plane-based registration methods, L2M-Reg, along with PLADE and Scantra, all utilize plane features to estimate the optimal transformation. However, their performance differs significantly in the context of building-level registration tasks, mainly attributable to their implementation.

The design of PLADE and Scantra lies in extracting a large number of planes prior to establishing correspondences using geometric descriptors. While effective in general urban scenes, this strategy proves unsuitable for individual buildings, which typically

contain a limited number of planes with diverse orientations. In addition, their correspondence establishment heavily rely on rich geometric structures and distinctive features. This makes them less effective when applied to geometrically simplified or feature-sparse LoD2 models of individual buildings, accounting for their performance in the evaluated scenarios.

5.3. Explanation of Using Road Model in the Street Building Dataset

In the Street Building dataset, a local road model is used instead of DTM to provide constraints in the vertical direction. This choice is motivated by two main factors. First, increasingly detailed ground and road models—such as high-definition maps for autonomous driving—are becoming available for local areas. Although their spatial coverage is currently limited, these datasets often offer higher accuracy than DTM derived from ALS and can serve as more reliable sources of absolute elevation. Second, the effectiveness of L2M-Reg when using DTM data has already been demonstrated based on the TUM0501 and Pinakothek datasets. Owing to the 2D–3D decoupled parameter estimation strategy introduced in this study, the estimation of vertical translation parameters does not affect other transformation parameters. Therefore, using road model in the Street Building dataset further illustrates the adaptability of L2M-Reg.

While a slight difference in vertical accuracy is observed between L2M-Reg and the best-performing baseline (GICP) in the quantitative results (see Tables 3 and 4), this discrepancy is primarily attributed to redundant layers within the used road model, which distort the accuracy evaluation. Provided higher-quality road data in the future, L2M-Reg can readily adapt to such data sources.

5.4. Limitations

As with most fine registration methods, L2M-Reg also requires an initial alignment. Developing a one-step solution that removes the dependency on coarse registration will be an important direction for future research.

Additionally, L2M-Reg assumes that the plinth regions are at least partially visible in the point clouds and not completely obstructed by vegetation or vehicles during data acquisition. Although a complete occlusion is very uncommon in practical scenarios, this assumption should be explicitly acknowledged.

6. Conclusion

This paper introduces L2M-Reg, a plane-based LiDAR-to-Model registration method tailored for individual buildings, with a particular focus on addressing the inherent uncertainty in LoD2 models. The key innovations of L2M-Reg are threefold. First, it considers uncertainty of LoD2 models, which serves as reference data, and introduces automated algorithms to identify representative regions and extract plane segments. Second, it introduces the concept of pseudo-planes in GHM and employs a 2D–3D decoupled parameter estimation strategy, which effectively mitigates the influence of low-reliability vertical model data on the estimation of horizontal parameters. Third, it maximizes the use of embedded semantic information in LoD2 models to enhance both the efficiency and reliability of plane correspondence establishment.

L2M-Reg was evaluated against leading solutions, including both ICP- and plane-based methods, across three real-world datasets. Experimental results show that L2M-Reg outperforms them in both accuracy and computational efficiency. Overall, L2M-Reg

contributes toward bridging the gap in uncertainty-aware LiDAR-to-Model fine registration at the building level.

Accurate and efficient LiDAR-to-Model registration remains an open research challenge. Developing a one-step registration method that eliminates dependence on coarse registration represents a promising direction for future work. Additionally, extending the current L2M-Reg to support seamless registration across both indoor and outdoor environments presents another important avenue for further research.

CRedit authorship contribution statement

Ziyang Xu: Conceptualization, Methodology, Software, Validation, Investigation, Writing – review & editing, Writing – original draft, Visualization. **Benedikt Schwab:** Conceptualization, Resources, Data Curation, Writing - original draft, Writing – review & editing. **Yihui Yang:** Conceptualization, Validation, Visualization, Writing - original draft, Writing – review & editing. **Thomas H. Kolbe:** Supervision, Writing - Review & Editing. **Christoph Holst:** Supervision, Writing - Review & Editing, Funding acquisition, Project administration.

Declaration of competing interest

The authors declare that they have no known competing financial interests or personal relationships that could have appeared to influence the work reported in this paper.

Acknowledgments

This research was funded by TUM Georg Nemetschek Institute of Artificial Intelligence for the Built World, project "NERF2BIM", PI Christoph Holst. Many thanks to the City of Munich / GeodatenService for supporting this research.

Data and code availability

The datasets used in this paper and the implementation of code for L2M-Reg will be publicly available upon acceptance.

References

- ASAM, 2024. OpenDRIVE V1.8.1 User Guide. <https://www.asam.net/standards/detail/opendrive/> (accessed 2 July 2025).
- Besl, P.J., McKay, N.D., 1992. Method for registration of 3-D shapes, in: Sensor Fusion IV: Control Paradigms and Data Structures, Spie. pp. 586–606.
- Biljecki, F., Stoter, J., Ledoux, H., Zlatanova, S., Çöltekin, A., 2015. Applications of 3D city models: State of the art review. ISPRS International Journal of Geo-Information 4, 2842–2889.
- Bosché, F., 2012. Plane-based registration of construction laser scans with 3D/4D building models. Advanced Engineering Informatics 26, 90–102.

- Bueno, M., Bosché, F., González-Jorge, H., Martínez-Sánchez, J., Arias, P., 2018. 4-plane congruent sets for automatic registration of as-is 3D point clouds with 3D BIM models. *Automation in Construction* 89, 120–134.
- Censi, A., 2008. An ICP variant using a point-to-line metric, in: 2008 IEEE International Conference on Robotics and Automation, IEEE. pp. 19–25.
- Chen, S., Nan, L., Xia, R., Zhao, J., Wonka, P., 2019. PLADE: A plane-based descriptor for point cloud registration with small overlap. *IEEE Transactions on Geoscience and Remote Sensing* 58, 2530–2540.
- Chetverikov, D., Svirko, D., Stepanov, D., Krsek, P., 2002. The trimmed iterative closest point algorithm, in: 2002 International Conference on Pattern Recognition, IEEE. pp. 545–548.
- Di, J., Zobeidi, E., Koppel, A., Atanasov, N., 2022. Distributed Gaussian process mapping for robot teams with time-varying communication, in: 2022 American Control Conference (ACC), IEEE. pp. 4458–4464.
- Diakite, A.A., Zlatanova, S., 2020. Automatic geo-referencing of BIM in GIS environments using building footprints. *Computers, Environment and Urban Systems* 80, 101453.
- Dold, C., Brenner, C., 2006. Registration of terrestrial laser scanning data using planar patches and image data. *The International Archives of the Photogrammetry, Remote Sensing and Spatial Information Sciences; XXXVI-Part 5* 36, 78–83.
- Feng, D., Wang, Z., Zhou, Y., Rosenbaum, L., Timm, F., Dietmayer, K., Tomizuka, M., Zhan, W., 2021. Labels are not perfect: Inferring spatial uncertainty in object detection. *IEEE Transactions on Intelligent Transportation Systems* 23, 9981–9994.
- Foschi, R., Fallavollita, F., Apollonio, F.I., 2024. Quantifying uncertainty in hypothetical 3D reconstruction—a user-independent methodology for the calculation of average uncertainty. *Heritage* 7, 4440–4454.
- Goebbels, S., Pohle-Fröhlich, R., Pricken, P., 2019. Iterative closest point algorithm for accurate registration of coarsely registered point clouds with CityGML models. *ISPRS Annals of the Photogrammetry, Remote Sensing and Spatial Information Sciences IV-2/W5*, 201–208.
- Gröger, G., Plümer, L., 2012. CityGML–interoperable semantic 3D city models. *ISPRS Journal of Photogrammetry and Remote Sensing* 71, 12–33.
- Holst, C., Artz, T., Kuhlmann, H., 2014. Biased and unbiased estimates based on laser scans of surfaces with unknown deformations. *Journal of applied geodesy* 8, 169–184.
- Holst, C., Medic, T., Nothnagel, A., Kuhlmann, H., 2019. Analyzing shape deformation and rigid body movement of structures using commonly misaligned terrestrial laser scanners: The radio telescope case, in: Proceedings of the 4th Joint International Symposium on Deformation Monitoring (JISDM), Athens, Greece, pp. 15–17.

- Jeddoub, I., Nys, G.A., Hajji, R., Billen, R., 2023. Digital twins for cities: Analyzing the gap between concepts and current implementations with a specific focus on data integration. *International Journal of Applied Earth Observation and Geoinformation* 122, 103440.
- Kada, M., McKinley, L., 2009. 3D building reconstruction from LiDAR based on a cell decomposition approach. *International Archives of Photogrammetry, Remote Sensing and Spatial Information Sciences XXXVIII-3/W4*, 47–52.
- Kaiser, T., Clemen, C., Maas, H.G., 2022. Automatic co-registration of photogrammetric point clouds with digital building models. *Automation in Construction* 134, 104098.
- Kalenjuk, S., Lienhart, W., 2022. A method for efficient quality control and enhancement of mobile laser scanning data. *Remote Sensing* 14, 857.
- Kensek, K.M., 2007. Survey of methods for showing missing data, multiple alternatives, and uncertainty in reconstructions. *CSA Newsletter* 19.
- Ketzler, B., Naserentin, V., Latino, F., Zangelidis, C., Thuvander, L., Logg, A., 2020. Digital twins for cities: A state of the art review. *Built Environment* 46, 547–573.
- Kolbe, T.H., Kutzner, T., Smyth, C.S., Nagel, C., Roensdorf, C., Heazel, C., 2021. OGC City Geography Markup Language (CityGML) Part 1: Conceptual Model Standard v3.0.
- Kulmer, D., Leitenstern, M., Weinmann, M., Lienkamp, M., 2025. OpenLiDARMap: Zero-drift point cloud mapping using map priors. *arXiv preprint arXiv:2501.11111* .
- Kumar, K., Labetski, A., Ledoux, H., Stoter, J., 2019. An improved LOD framework for the terrains in 3D city models. *ISPRS Annals of the Photogrammetry, Remote Sensing and Spatial Information Sciences* 4, 75–82.
- Kutsch, A., Margreiter, M., Bogenberger, K., 2024. TUMDOT–MUC: Data collection and processing of multimodal trajectories collected by aerial drones. *Data Science for Transportation* 6, 15.
- Lague, D., Brodu, N., Leroux, J., 2013. Accurate 3D comparison of complex topography with terrestrial laser scanner: Application to the Rangitikei canyon (NZ). *ISPRS Journal of Photogrammetry and Remote Sensing* 82, 10–26.
- Landes, T., Heissler, M., Koehl, M., Benazzi, T., Nivola, T., 2019. Uncertainty visualization approaches for 3D models of castles restituted from archeological knowledge. *The International Archives of the Photogrammetry, Remote Sensing and Spatial Information Sciences* 42, 409–416.
- Liu, Z., Blut, C., Blankenbach, J., 2024. Automatic 3D model registration for global localization based on publicly available georeferenced CityGML data. *The International Archives of the Photogrammetry, Remote Sensing and Spatial Information Sciences XLVIII-4/W11-2024*, 65–71.
- Low, K.L., 2004. Linear least-squares optimization for point-to-plane ICP surface registration. *Chapel Hill, University of North Carolina* 4, 1–3.

- Lucks, L., Klingbeil, L., Plümer, L., Dehbi, Y., 2021. Improving trajectory estimation using 3D city models and kinematic point clouds. *Transactions in GIS* 25, 238–260.
- Ma, G., Wei, H., 2023. A novel sketch-based framework utilizing contour cues for efficient point cloud registration. *IEEE Transactions on Geoscience and Remote Sensing* 61, 1–16.
- Macay Moreia, J., Nex, F., Agugiaro, G., Remondino, F., Lim, N.J., 2013. From DSM to 3D building models: A quantitative evaluation. *The International Archives of the Photogrammetry, Remote Sensing and Spatial Information Sciences* 40, 213–219.
- Meyer, T., Brunn, A., Stilla, U., 2022. Change detection for indoor construction progress monitoring based on BIM, point clouds and uncertainties. *Automation in Construction* 141, 104442.
- Mikhail, E.M., Ackermann, F.E., 1976. Observations and least squares. *IEP Series in Civil Engineering*, IEP.
- Monasse, P., Djahel, R., Vallet, B., 2023. Registration for urban modeling based on linear and planar features, in: *2023 11th European Workshop on Visual Information Processing (EUVIP)*, IEEE. pp. 1–8.
- Paz, D., Zhang, H., Li, Q., Xiang, H., Christensen, H.I., 2020. Probabilistic semantic mapping for urban autonomous driving applications, in: *2020 IEEE/RSJ International Conference on Intelligent Robots and Systems (IROS)*, IEEE. pp. 2059–2064.
- Potter, K., Rosen, P., Johnson, C.R., 2012. From quantification to visualization: A taxonomy of uncertainty visualization approaches, in: *Uncertainty Quantification in Scientific Computing: 10th IFIP WG 2.5 Working Conference, WoCoUQ 2011*, Boulder, CO, USA, August 1-4, 2011, Revised Selected Papers, Springer. pp. 226–249.
- Qiao, J., Butt, J.A., 2023. Self-calibration of terrestrial laser scanner using a M3C2-based planar patch algorithm. *ISPRS Journal of Photogrammetry and Remote Sensing* 197, 335–345.
- Roschlaub, R., Batscheider, J., 2016. An inspire-konform 3D building model of Bavaria using cadastre information, LiDAR and image matching. *The International Archives of the Photogrammetry, Remote Sensing and Spatial Information Sciences* XLI-B4, 747–754.
- Rusinkiewicz, S., Levoy, M., 2001. Efficient variants of the ICP algorithm, in: *Proceedings Third International Conference on 3-D digital Imaging and Modeling*, IEEE. pp. 145–152.
- Rusu, R.B., Cousins, S., 2011. 3D is here: Point Cloud Library (PCL), in: *2011 IEEE International Conference on Robotics and Automation (ICRA)*, IEEE, Shanghai, China. pp. 1–4.
- Schuegraf, P., Shan, J., Bittner, K., 2024. PLANES4LOD2: Reconstruction of LoD-2 building models using a depth attention-based fully convolutional neural network. *ISPRS Journal of Photogrammetry and Remote Sensing* 211, 425–437.

- Schwab, B., Beil, C., Kolbe, T.H., 2020. Spatio-semantic road space modeling for vehicle–pedestrian simulation to test automated driving systems. *Sustainability* 12, 3799.
- Segal, A., Haehnel, D., Thrun, S., 2009. Generalized-ICP, in: *Robotics: science and systems*, Seattle, WA. p. 435.
- Shao, J., Yao, W., Wang, P., He, Z., Luo, L., 2024. Urban GeoBIM construction by integrating semantic LiDAR point clouds with as-designed BIM models. *IEEE Transactions on Geoscience and Remote Sensing* 62, 1–12.
- Sheik, N.A., Deruyter, G., Veelaert, P., 2022a. Plane-based robust registration of a building scan with its BIM. *Remote Sensing* 14, 1979.
- Sheik, N.A., Veelaert, P., Deruyter, G., 2022b. Registration of building scan with IFC-based BIM using the corner points. *Remote Sensing* 14, 5271.
- Wujanz, D., Schaller, S., Gielsdorf, F., Gründig, L., 2018. Plane-based registration of several thousand laser scans on standard hardware. *The International Archives of the Photogrammetry, Remote Sensing and Spatial Information Sciences* 42, 1207–1212.
- Wysocki, O., Schwab, B., Beil, C., Holst, C., Kolbe, T.H., 2024. Reviewing open data semantic 3D city models to develop novel 3D reconstruction methods. *The International Archives of the Photogrammetry, Remote Sensing and Spatial Information Sciences* 48, 493–500.
- Wysocki, O., Schwab, B., Biswanath, M.K., Zhang, Q., Zhu, J., Froech, T., Heerama-glore, M., Hijazi, I., Kanna, K., Pechinger, M., et al., 2025. TUM2TWIN: Introducing the large-scale multimodal urban digital twin benchmark dataset. *arXiv preprint arXiv:2505.07396* .
- Wysocki, O., Xu, Y., Stilla, U., 2021. Unlocking point cloud potential: Fusing mls point clouds with semantic 3D building models while considering uncertainty. *ISPRS Annals of the Photogrammetry, Remote Sensing and Spatial Information Sciences VIII-4/W2-2021*, 45–52.
- Xu, Y., Boerner, R., Yao, W., Hoegner, L., Stilla, U., 2017. Automated coarse registration of point clouds in 3D urban scenes using voxel based plane constraint. *ISPRS annals of the photogrammetry, remote sensing and spatial information sciences* 4, 185–191.
- Xu, Y., Boerner, R., Yao, W., Hoegner, L., Stilla, U., 2019. Pairwise coarse registration of point clouds in urban scenes using voxel-based 4-planes congruent sets. *ISPRS journal of photogrammetry and remote sensing* 151, 106–123.
- Xu, Y., Stilla, U., 2021. Toward building and civil infrastructure reconstruction from point clouds: A review on data and key techniques. *IEEE Journal of Selected Topics in Applied Earth Observations and Remote Sensing* 14, 2857–2885.
- Xu, Z., Hackl, M., Holst, C., 2025. PL4U: Automated plane-based uncertainty evaluation and reduction method for indoor mobile laser scanning systems. *ISPRS Journal of Photogrammetry and Remote Sensing* 228, 467–488.

- Yang, Y., Holst, C., 2025. Piecewise-ICP: Efficient and robust registration for 4D point clouds in permanent laser scanning. *ISPRS Journal of Photogrammetry and Remote Sensing* 227, 481–500.
- Yang, Y., Schwieger, V., 2023. Supervoxel-based targetless registration and identification of stable areas for deformed point clouds. *Journal of Applied Geodesy* 17, 161–170.
- Zhu, J., Wysocki, O., Holst, C., Kolbe, T.H., 2024. Enriching thermal point clouds of buildings using semantic 3D building models. *ISPRS Annals of the Photogrammetry, Remote Sensing and Spatial Information Sciences X-4/W5-2024*, 341–348.
- Zou, Q., Sester, M., 2022. Uncertainty representation and quantification of 3D building models. *International Archives of the Photogrammetry, Remote Sensing and Spatial Information Sciences XLIII-B2-2022*, 335–341.
- Zuk, T., Carpendale, S., Glanzman, W.D., 2005. Visualizing temporal uncertainty in 3D virtual reconstructions., in: *VAST*, p. 6th.